Acta Crystallographica Section D
Biological Crystallography
ISSN 1399-0047

Crystallographic analysis of 1,2,3-trichloropropane biodegradation by the haloalkane dehalogenase DhaA31

Maryna Lahoda, Jeroen R. Mesters, Alena Stsiapanava, Radka Chaloupkova, Michal Kuty, Jiri Damborsky and Ivana Kuta Smatanova

Acta Cryst. (2014). D**70**, 209–217

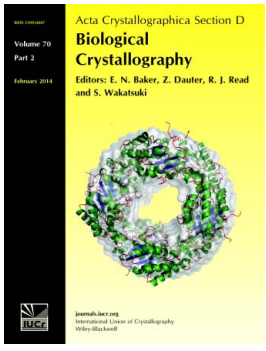

Acta Crystallographica Section D: Biological Crystallography welcomes the submission of papers covering any aspect of structural biology, with a particular emphasis on the structures of biological macromolecules and the methods used to determine them. Reports on new protein structures are particularly encouraged, as are structure–function papers that could include crystallographic binding studies, or structural analysis of mutants or other modified forms of a known protein structure. The key criterion is that such papers should present new insights into biology, chemistry or structure. Papers on crystallographic methods should be oriented towards biological crystallography, and may include new approaches to any aspect of structure determination or analysis. Papers on the crystallization of biological molecules will be accepted providing that these focus on new methods or other features that are of general importance or applicability.

Acta Crystallographica Section D
Biological Crystallography
ISSN 1399-0047

Crystallographic analysis of 1,2,3-trichloropropane biodegradation by the haloalkane dehalogenase DhaA31

Maryna Lahoda,[a,b] Jeroen R. Mesters,[c] Alena Stsiapanava,[b] Radka Chaloupkova,[d] Michal Kuty,[b,e] Jiri Damborsky[d] and Ivana Kuta Smatanova[b,e]*

[a]Institute of Complex Systems, FFPW and CENAKVA, University of South Bohemia in Ceske Budejovice, Zamek 136, 373 33 Nove Hrady, Czech Republic, [b]Faculty of Science, University of South Bohemia in Ceske Budejovice, Branisovska 31, 370 05 Ceske Budejovice, Czech Republic, [c]Institute of Biochemistry, Center for Structural and Cell Biology in Medicine, University of Lübeck, Ratzeburger Allee 160, 23538 Lübeck, Germany, [d]Loschmidt Laboratories, Department of Experimental Biology and Research Centre for Toxic Compounds in the Environment, Faculty of Science, Masaryk University Brno, Kamenice 5/A13, 625 00 Brno, Czech Republic, and [e]Institute of Nanobiology and Structural Biology GCRC, Academy of Science of the Czech Republic, Zamek 136, 373 33 Nove Hrady, Czech Republic

Correspondence e-mail: ivanaks@seznam.cz

Received 23 May 2013
Accepted 23 September 2013

PDB references: DhaA31, substrate-free, 3rk4; complex with TCP, 4fwb; wild-type DhaA, 4hzg

Haloalkane dehalogenases catalyze the hydrolytic cleavage of carbon–halogen bonds, which is a key step in the aerobic mineralization of many environmental pollutants. One important pollutant is the toxic and anthropogenic compound 1,2,3-trichloropropane (TCP). Rational design was combined with saturation mutagenesis to obtain the haloalkane dehalogenase variant DhaA31, which displays an increased catalytic activity towards TCP. Here, the 1.31 Å resolution crystal structure of substrate-free DhaA31, the 1.26 Å resolution structure of DhaA31 in complex with TCP and the 1.95 Å resolution structure of wild-type DhaA are reported. Crystals of the enzyme–substrate complex were successfully obtained by adding volatile TCP to the reservoir after crystallization at pH 6.5 and room temperature. Comparison of the substrate-free structure with that of the DhaA31 enzyme–substrate complex reveals that the nucleophilic Asp106 changes its conformation from an inactive to an active state during the catalytic cycle. The positions of three chloride ions found inside the active site of the enzyme indicate a possible pathway for halide release from the active site through the main tunnel. Comparison of the DhaA31 variant with wild-type DhaA revealed that the introduced substitutions reduce the volume and the solvent-accessibility of the active-site pocket.

1. Introduction

Halogenated compounds can serve as a carbon and energy source for certain aerobic microorganisms. Such organisms have specifically developed a variety of enzyme systems to degrade these compounds. On the other hand, many synthetically prepared halogenated chemicals, which represent important environmental pollutants, such as 1,2-dichloroethane, 1,2-dichloropropane and 1,2,3-trichloropropane, are not easily biodegraded (Janssen *et al.*, 2005). Haloalkane dehalogenases have the potential to convert these halogenated hydrocarbons to the corresponding alcohols by hydrolytic cleavage of their carbon–halogen bonds (Pries, van den Wijngaard *et al.*, 1994; Pries, van der Ploeg *et al.*, 1994; Bosma *et al.*, 2002). The first haloalkane dehalogenase reported to have detectable activity towards 1,2,3-trichloropropane (TCP) was DhaA, which was isolated from the Gram-positive bacterium *Rhodococcus rhodochrous* NCIMB 13064 (Kulakova *et al.*, 1997). Wild-type DhaA slowly converts (k_{cat} = 0.08 s^{-1}) the toxic and potentially carcinogenic TCP to 2,3-dichloropropane-1-ol (DCL) under laboratory conditions (Schindler *et al.*, 1999; Bosma *et al.*, 1999; Pavlova *et al.*, 2009). The conversion of TCP to DCL (k_{cat} = 0.005 s^{-1}) using the same reaction mechanism, but significantly more slowly, has been reported for the related haloalkane dehalogenase LinB

(Monincová *et al.*, 2007). The haloalkane dehalogenases consist of two domains: a main α/β-hydrolase domain and an α-helical cap domain. The active site of haloalkane dehalogenases is located between the two domains in a hydrophobic cavity connected to the protein surface by two major access tunnels designated the main tunnel and the slot tunnel; three additional transient tunnels have been identified by molecular modelling (Klvana *et al.*, 2009). Ligands can move freely between the buried active site and the surrounding solvent through the two major access tunnels. The dehalogenation reaction catalyzed by haloalkane dehalogenases takes place in the buried active site. The halogenated substrate binds to form the substrate–enzyme complex and the nucleophilic residue Asp106 attacks an sp^3-hybridized C atom of the bound substrate, resulting in the formation of a covalent alkyl-enzyme intermediate by cleavage of the carbon–halogen bond and release of the halide ion. The alkyl-enzyme intermediate is subsequently hydrolyzed by a water molecule activated by the catalytic base His272 (Schindler *et al.*, 1999; Otyepka *et al.*, 2007; Pavlova *et al.*, 2009).

Several variants of DhaA have been constructed and characterized with the goal of improving the enzymatic kinetic properties for TCP conversion (Banás *et al.*, 2006; Bosma *et al.*, 2002; Gray *et al.*, 2001; Pavlova *et al.*, 2009). The most successful variant, DhaA31, exhibited a 32-fold higher catalytic activity and a 26-fold higher catalytic efficiency for TCP at an optimal pH value of 8.6 and 37°C than the wild-type enzyme (Pavlova *et al.*, 2009). This variant carries five amino-acid substitutions: I135F, C176Y, V245F, L246I and Y273F. The C176Y variation, which is located in the cap domain, was suggested to modify the mouth of the main tunnel that connects the buried active site to surrounding solvent. With the Y273F variation (located in the active site), a hydrogen bond to the main-chain carbonyl O atom of Asn41 is lost. V245F is located in the main tunnel and I135F and L246I are located in the slot tunnel and in the active site, respectively (Bosma *et al.*, 2002; Pavlova *et al.*, 2009).

In this study, the DhaA31 variant was crystallized in a substrate-free form and vapour-soaked in the presence of TCP at pH 6.5 and various temperatures. An analogous crystallographic analysis has previously been carried out using the haloalkane dehalogenase DhlA from *Xanthobacter autotrophicus* GJ10 (Verschueren, Seljée *et al.*, 1993), in which different stages of the reaction pathway of the enzyme were trapped by varying the pH and temperature during soaking experiments with 1,2-dichoroethane. At pH 5.0 and 4°C the enzyme–substrate complex was captured. Increasing the temperature resulted in the accumulation of a covalently bound intermediate in the active site and increasing the pH to 6.2 allowed the release of the alcohol, while the chloride ion was bound more stably than at higher pH values (Verschueren, Kingma *et al.*, 1993*b*). At pH 8.2, an optimal condition for catalysis, significant movement in the position of the catalytic residues was observed. The catalytic histidine was mostly neutral, which results in loss of the salt bridge between the catalytic base and the nucleophile, as observed in the pH 6.2 structure. This left the negatively charged aspartate side chain ready to perform a nucleophilic attack on the C atom of the substrate molecule (Verschueren, Kingma *et al.*, 1993*a*; Verschueren, Seljée *et al.*, 1993).

We analyzed and compared the crystal structure of DhaA31 in its free form with those of wild-type DhaA and the DhaA31–substrate complex. This comparison revealed two alternative conformations of the nucleophilic residue Asp106 in the DhA31–TCP complex and enabled the identification of seven chlorine-atom/chloride-ion locations within the active site. The position and spatial arrangement of three of these atoms/ions can be explained by modelling with a TCP molecule. The DhaA31 variant also carries five amino-acid substitutions that reduce the volume of the active-site cavity and its accessibility to water molecules, which may provide an explanation for the higher catalytic efficiency with TCP.

2. Materials and methods

2.1. Protein crystallization

The standard sitting-drop vapour-diffusion technique (Ducruix & Giegé, 1999) was performed in CombiClover crystallization plates (EBS plate, Emerald BioStructures, Washington, USA) at 277 K. Three-dimensional crystals of DhaA31 were grown from 2 µl droplets consisting of equal volumes of protein solution (7 mg ml^{-1} in 50 m*M* Tris–HCl buffer pH 7.5) and reservoir solution [29%(*w*/*v*) PEG 4000, 100 m*M* MES–NaOH buffer pH 6.4] equilibrated against the reservoir solution. The final pH of the crystallization composition was 6.5, which should in principle help to capture an enzyme–substrate complex, as demonstrated by Verschueren, Kingma *et al.* (1993*b*). The crystals grew to final dimensions of $0.28 \times 0.19 \times 0.13$ mm in three weeks. For complex formation, crystals were placed over 800 µl reservoir solution with 50 µl TCP and left at room temperature for 6 h to ensure slow penetration of the substrate into the crystals by TCP vapour diffusion, thereby avoiding the crystal destruction that takes place on direct soaking (Lahoda *et al.*, 2011). Crystals of wild-type DhaA were obtained in 5 d by mixing 1 µl protein solution at a concentration of 11 mg ml^{-1} in 50 µl Tris–HCl buffer pH 7.5 with an equal volume of precipitant solution composed of 39%(*w*/*v*) PEG 4000, 8%(*v*/*v*) TCP, 100 m*M* sodium acetate pH 8.8, giving a final pH value of 7.8. The drops were equilibrated over 700 µl reservoir solution (Stsiapanava *et al.*, 2011). Prior to data collection, the crystals of wild-type DhaA were soaked in a solution consisting of 25%(*v*/*v*) glycerol, 20% PEG 4000, 4% TCP, 50 m*M* sodium acetate pH 7.2 and were flash-cooled in liquid nitrogen.

2.2. Data collection

Diffraction data for substrate-free DhaA31 and DhaA31 in complex with TCP were collected on beamline X12 of the EMBL Outstation at DESY, Hamburg equipped with a MAR CCD 225 mm detector at a fixed wavelength of 1.033 Å. Crystals were mounted directly in a nylon loop (Hampton Research, Aliso Viejo, USA; Teng, 1990) and flash-cooled in a cold nitrogen stream at 100 K without additional

cryoprotection. The presence of TCP may have aided the flash-cooling process, preventing ice rings during data collection. DhaA31 data sets were collected in two steps. 120 low-resolution images (50–2.89 Å) were recorded with an oscillation angle of 3° and a crystal-to-detector distance of 300 mm. A high-resolution data set of 360 images (50–1.31 Å resolution) was collected with an oscillation angle of 1° and a crystal-to-detector distance of 100 mm. For DhaA31 in complex with TCP, 400 high-resolution images (50–1.26 Å resolution) were collected with a 0.5° oscillation angle and a crystal-to-detector distance of 100 mm. This was followed by the collection of 130 image frames with a 1.5° oscillation angle and a crystal-to-detector distance of 300 mm. Data for both crystals were integrated and scaled using the *HKL*-2000 program package (Otwinowski & Minor, 1997).

Diffraction data for wild-type DhaA were collected on beamline 14.2 at the BESSY II electron-storage ring (Mueller *et al.*, 2012) operated by the Joint Berlin MX-Laboratory (Berlin-Adlershof, Germany). Experiments were performed at a single wavelength of 1.9 Å using a Rayonix 225 mm CCD detector. A single data set (22–1.85 Å resolution) consisting of 360 images was collected with an oscillation angle of 1° per image and a crystal-to-detector distance of 60 mm. The data were indexed and integrated using *XDS* (Kabsch, 1993, 2010*a*,*b*) and scaled using *SCALA* from the *CCP*4 program suite (Winn *et al.*, 2011). The data-collection statistics are summarized in Table 1.

Table 1
Data-collection and refinement statistics.

	DhaA31	DhaA31–TCP	DhaA
Data collection			
Resolution range (Å)	50–1.31 (1.35–1.31)	50–1.26 (1.27–1.26)	22–1.85 (1.94–1.85)
Space group	*P*1	*P*1	*P*1
Unit-cell parameters (Å, °)	*a* = 42.55, *b* = 44.37, *c* = 46.41, α = 115.3, β = 98.5, γ = 109.5	*a* = 42.49, *b* = 44.39, *c* = 46.53, α = 115.3, β = 97.7, γ = 109.5	*a* = 44.77, *b* = 44.47, *c* = 46.51, α = 115.3, β = 97.8, γ = 109.2
Unique reflections (observed)	73847	74995	20934
Average multiplicity	4.3	2.4	3.7
Completeness (%)	94.6 (90.3)	92.4 (82.7)	87.8 (81.5)
R_{merge}†	0.044 (0.081)	0.033 (0.061)	0.158 (0.568)
$\langle I\rangle/\langle\sigma(I)\rangle$	35.6 (18.3)	41.1 (17.6)	5.3 (2.0)
Wilson *B* factor (Å^2)	8.24	8.60	20.44
Refinement			
No. of reflections used for refinement	61990	69189	17017
Maximum resolution (Å)	1.31	1.26	1.95
R_{work}‡/R_{free}§	0.128/0.160	0.135/0.164	0.216/0.273
No. of non-H atoms	2855	2824	2645
No. of protein atoms	2469	2461	2412
No. of ligand atoms	1	10	1
No. of chloride ions	1	4	1
No. of water molecules	385	353	232
Average *B* value (Å^2)	11.23	11.43	19.87
R.m.s. deviations from ideal¶			
Bond lengths (Å)	0.012	0.012	0.014
Bond angles	0.028 Å	0.029 Å	1.665°
Clashscore [percentile]††	3.25 [97]	4.07 [91]	5.44 [96]
Poor rotamers†† (%)	2.40	2.40	2.38
Ramachandran statistics of φ/ψ angles†† (%)			
Most favoured	97.24	97.24	96.92
Outliers			0.34
PDB code	3rk4	4fwb	4hzg

† $R_{merge} = \sum_{hkl}\sum_i |I_i(hkl) - \langle I(hkl)\rangle|/\sum_{hkl}\sum_i I_i(hkl)$, where $I_i(hkl)$ is the intensity of the *i*th measurement of reflection *hkl* and $\langle I(hkl)\rangle$ is the average intensity of the reflection. ‡ $R_{work} = \sum_{hkl} ||F_{obs}| - |F_{calc}||/\sum_{hkl}|F_{obs}|$. § R_{free} was monitored using 5% of the reflection data that were excluded from refinement. ¶ Engh and Huber parameters (Engh & Huber, 1991, 2001). †† According to *MolProbity* (Chen *et al.*, 2010).

2.3. Structure solution and refinement

The structures of DhaA31, of its complex with TCP and of wild-type DhaA were solved by the molecular-replacement method using *MOLREP* (Vagin & Teplyakov, 2010). The structure of haloalkane dehalogenase DhaA variant C176Y (PDB entry 3fbw; Stsiapanava *et al.*, 2010) was used as the search model. The structures of DhaA31 were refined employing *SHELXL* (Sheldrick, 2008). The *Coot* package was used for manual model building (Emsley *et al.*, 2010). After several rounds of structure refinement omitting all ligands at the active site (henceforth termed the largely refined structure), the $|F_o| - |F_c|$ Fourier difference peaks in the active site were finally interpreted. The difference density in the active site of the substrate-free DhaA31 structure was interpreted as a chloride ion from the anomalous difference maxima and the typical distances of Cl$^-$–HN contacts. The structure of DhaA31 in complex with substrate displays electron density for one 1,2,3-trichloropropane molecule and four additional positions for chloride-ion binding as shown by analysis of the anomalous difference maxima. Except for water O atoms (see §8.4 of the *SHELXL*-97 manual; http://shelx.uni-ac.gwdg.de/SHELX/shelx97.pdf), anisotropic atomic displacement parameters were used in the refinement. Compared with standard isotropic refinement, the combined isotropic/anisotropic ADP refinement resulted in lower *R* and R_{free} values (from *R* = 0.234 and R_{free} = 0.257 to *R* = 0.128 and R_{free} = 0.160 for DhaA31 and from *R* = 0.251 and R_{free} = 0.279 to *R* = 0.135 and R_{free} = 0.164 for DhaA31 in complex with TCP).

Restrained refinement of wild-type DhaA was performed in *REFMAC*5 (Murshudov *et al.*, 2011) and model building was performed in *Coot*. The atomic displacement parameters of all protein and water O atoms and the chloride ion were refined isotropically. Structure-refinement statistics are presented in Table 1.

2.4. Model validation and deposition

Structural models were assessed with respect to experimental data using *SFCHECK* (Vaguine *et al.*, 1999). Geometric parameters were validated by *Coot* (Emsley *et al.*,

2010) and *MolProbity* (Chen *et al.*, 2010). 90.0% of the residues in the substrate-free DhaA31 structure and 89.6% of the residues in the DhaA31–TCP complex are located in the 'core' region of the Ramachandran plot. In both structures, two residues are located in the 'generously allowed' region. These Ramachandran outliers with clear electron densities are the catalytic residue Asp106 and the variant residue Phe245, which are located in the active site and in the main tunnel, respectively. In the case of wild-type DhaA, 96.7% of the residues were in the most favoured regions of the Ramachandran plot and 100.0% of the residues were in allowed regions. The substrate-free DhaA31 structure, the DhaA31–TCP complex structure and the wild-type DhaA structure were assigned PDB codes 3rk4, 4fwb and 4hzg, respectively. The volumes of the active-site cavities were calculated using the 3*V* server with the following settings (Voss & Gerstein, 2010): grid resolution of 0.5 Å, outer probe radius of 3 Å and inner probe radius of 1.4 Å. The van der Waals volume of the TCP molecule was calculated using the Geometry plugin of *Marvin* 5.11.1 (ChemAxon, Budapest).

3. Results and discussion

3.1. Overall structure of the DhaA31 protein variant

The structure of wild-type haloalkane dehalogenase DhaA from *R. rhodochrous* NCIMB 13064 has previously been described by Newman *et al.* (1999). For both structures of the DhaA31 protein variant, electron density was clearly visible for amino-acid residues 4–295. Identically to the wild-type enzyme, the globular structure of DhaA31 displays the general dehalogenase fold consisting of two domains (Fig. 1; Holmquist, 2000; Chovancová *et al.*, 2007). The main domain with the α/β-hydrolase fold consists of an eight-stranded β-sheet surrounded by six α-helices (secondary-structure elements $\beta1$–$\beta2$–$\beta3$–$\alpha1$–$\beta4$–$\alpha2$–$\beta5$–$\alpha3$–$\beta6$–$\alpha8$–$\beta7$–$\alpha9$–$\beta8$–$\alpha10$). The second domain, called the cap domain, is sequentially inserted into the main domain between $\beta6$ and $\alpha8$, and is composed of five α-helices ($\alpha4$–$\alpha5'$–$\alpha5$–$\alpha6$–$\alpha7$). The active site is located between the main domain and the cap domain. The catalytic residues forming the catalytic pentad, Asn41, Asp106, Trp107, Glu130 and His272, are located in this cavity (Chovancová *et al.*, 2007; Stsiapanava *et al.*, 2010).

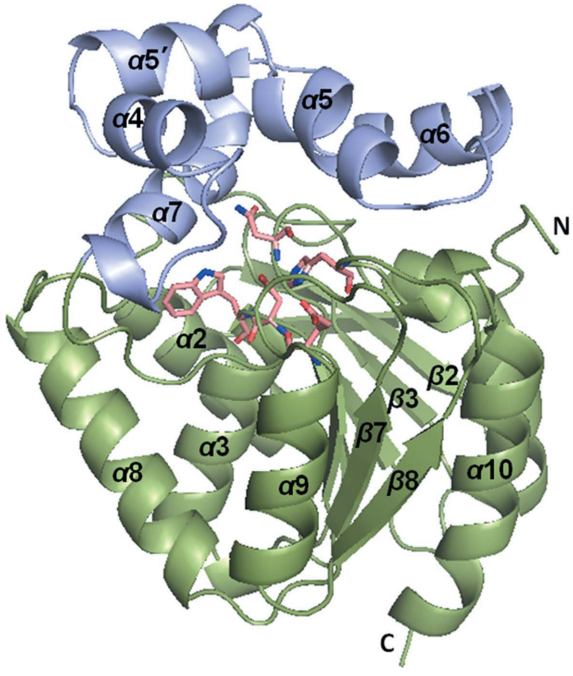

Figure 1
Cartoon representation of the DhaA31 structure. The α/β-hydrolase core domain is shown in green; the helical cap domain is shown in blue. Catalytic pentad residues are shown in magenta stick representation. Figures were prepared using *PyMOL* (DeLano, 2002).

3.2. Analysis of the active site

The active-site cavity of the largely refined substrate-free DhaA31 structure contained an $F_o - F_c$ difference electron-density peak (greater than 10σ above the mean) that was finally interpreted as a chloride ion. Coordinated to Asn41 $N^{\delta2}$ (at a distance of 3.33 Å) and Trp107 $N^{\varepsilon1}$ (3.32 Å), the chloride ion occupies the canonical halide-binding site (Fig. 2*a*) and most probably originates from the buffer solution. In addition, two water molecules were modelled close to the side chain of Asp106. The catalytic residue Asp106 displays a $C^{\alpha}-C^{\beta}-C^{\gamma}$ bond angle of 114.65°. The $N^{\delta1}$ atom of His272 interacts with the side chain of Glu130 (2.73 Å), and the $N^{\varepsilon2}$ atom of His272 interacts with the $O^{\delta1}$ atom (2.87 Å) of the side chain of Asp106. The $O^{\delta2}$ atom of Asp106 accepts hydrogen bonds from the main-chain amides of Asn41 (2.80 Å) and Trp107 (2.83 Å). This constellation is in good agreement with the hydrogen-bonding network observed in the structure of DhlA at low pH values (Verschueren, Kingma *et al.*, 1993*a*).

For crystals soaked with TCP, the largely refined DhaA31 structure exhibited four $F_o - F_c$ difference electron-density peaks greater than 10σ above the mean in the active site. In an effort to interpret the difference electron density, chloride ions, TCP substrate, alkyl-enzyme and product were modelled independently. We found that the three Cl atoms of the substrate 1,2,3-trichloropropane superimposed correctly with three of the four $F_o - F_c$ difference electron-density peaks. The 2,3-dichloropropane-1-ol product molecule does not superimpose well because of the shorter distance between the C and O atoms of the alcohol product (about 1.3 Å) compared with the C to Cl distance in the substrate molecule (about 1.8 Å). The largest $F_o - F_c$ difference electron-density peak (greater than 30σ above the mean) superimposed with the canonical halide-binding site. Nonetheless, we cannot fully exclude the concomitant existence of a near-attack and/or an alkyl-enzyme state. Unfortunately, modelling of these states had to be abandoned because of low occupancy. Finally, one chloride ion (Asn41 $N^{\delta2}$–Cl^-, 3.34 Å; Trp107 $N^{\varepsilon1}$–Cl^-, 3.27 Å; occupancy 1.0) in the canonical halide-binding site and one TCP molecule (occupancy 0.6) were modelled into the difference electron-density peaks. In addition, a water molecule (occupancy 0.4) and two conformations of the catalytic Asp106 residue were modelled with $C^{\alpha}-C^{\beta}-C^{\gamma}$ bond angles of 126.52° (alternative *A*, His272 $N^{\varepsilon2}$–Asp106 $O^{\delta1}$, 2.49 Å) and

106.93° (alternative *B*, His272 $N^{\varepsilon 2}$–Asp106 $O^{\delta 1}$, 3.11 Å). The unusual $C^{\alpha}-C^{\beta}-C^{\gamma}$ bond angle of alternative *A*, which is far outside the normally observed range and is stabilized by the formation of a strong ion pair with His272, may possibly play a role during catalysis. The occupancies of alternatives *A* and *B*, optimized by sampling steps of 0.1 and subsequent examination of the $F_o - F_c$ difference electron-density map, are 0.6 and 0.4, respectively (Fig. 2*b*). With the aforementioned interpretation of the difference electron-density map, three small parts of the initial peaks remained unsolved. Because of their very close proximity to the Cl-2 and Cl-3 atoms of the TCP substrate, these peaks were finally interpreted as low-occupancy (0.2–0.4) Cl atoms and we hypothesize that these may represent alternative conformations of low-occupancy substrate/product molecules or that these Cl atoms may reveal a possible route for halide release. Two distinct conformations of the nucleophile have previously been observed in the crystal structure of the haloalkane dehalogenase LinB solved at 0.95 Å resolution (Oakley *et al.*, 2004).

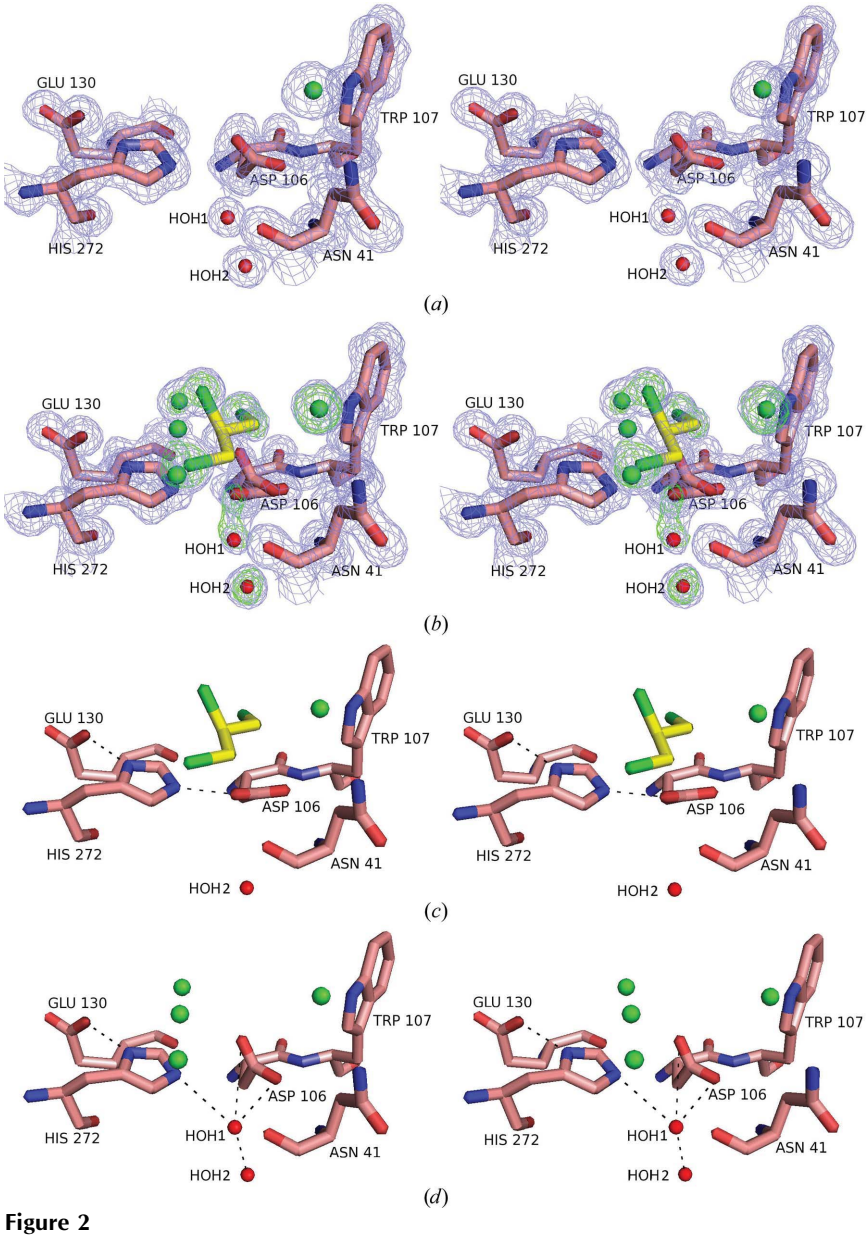

Figure 2
The active site of DhaA31. Active-site residues of substrate-free DhaA31 with a fixed position for Asp106 (*a*) and of DhaA31 in complex with TCP (*b*–*d*) are shown in stick representation. $2mF_o - DF_c$ electron-density maps are shown as a blue mesh (*a*, *b*) and an OMIT map ($mF_o - DF_c$ calculated omitting Cl atoms, TCP, water molecules and Asp106 alternative *A*) is shown as a green mesh (*b*). The electron-density map is contoured at 0.525 e Å^{-3} (1σ) and the OMIT map is contoured at 0.423 e Å^{-3} (3σ). TCP C and Cl atoms are coloured yellow and green, respectively. Green spheres represent chloride anions and red spheres represent O atoms of water molecules. (*c*, *d*) Alternative conformation *A* of the catalytic residue Asp106 in the post-attack configuration with the substrate (*c*) and alternative conformation *B* of the catalytic residue Asp106 with halide product leaving the active site (*d*).

A long-wavelength experiment (Mueller-Dieckmann *et al.*, 2005) was conducted to aid the location of Cl atoms in the structure of wild-type DhaA. One clear $F_o - F_c$ difference electron-density peak (greater than 10σ above the mean) was modelled as a chloride ion occupying the canonical halide-binding site. Additionally, three small $F_o - F_c$ difference electron-density peaks (less than 4.5σ above the mean) were located close to Cys176 but distally from Asp106. Modelling of a low-occupancy TCP molecule into the $F_o - F_c$ difference electron-density peaks was finally abandoned because the Cl atoms superposed incorrectly with the three $F_o - F_c$ difference electron-density peaks. Conceivably, the low affinity for TCP, the slightly basic pH value of the buffer used for mounting the crystal and substrate disorder owing to the large active-site cavity might explain why no complex was obtained.

3.3. Implications for the reaction mechanism

The crystal structure of the DhaA31–TCP complex displays a combination of two different states of the active-site cavity. One state is characterized by a post-attack conformation of Asp106 (alternative *A*, occupancy of 0.6). Here, the catalytic Asp106 must have already undergone a reaction cycle as shown by the absence of the catalytic water molecule (H_2O-1) used in the cleavage of the intermediate state (alkyl-enzyme), releasing the product 2,3-dichloropropane-1-ol (Fig. 2*c*). At this point, the His272 side chain most probably remains partly protonated owing to the pH of the crystallization drop (Verschueren, Seljée *et al.*, 1993) and as a consequence the $O^{\delta 1}$ atom of Asp106 interacts with the $N^{\varepsilon 2}$ atom of His272 at a distance of 2.53 Å, forming an ion pair (Fig. 3*c*). Apparently, the TCP substrate (occupancy of 0.6) in the active site did not replace the chloride product coordinated to the N atoms of the Asn41

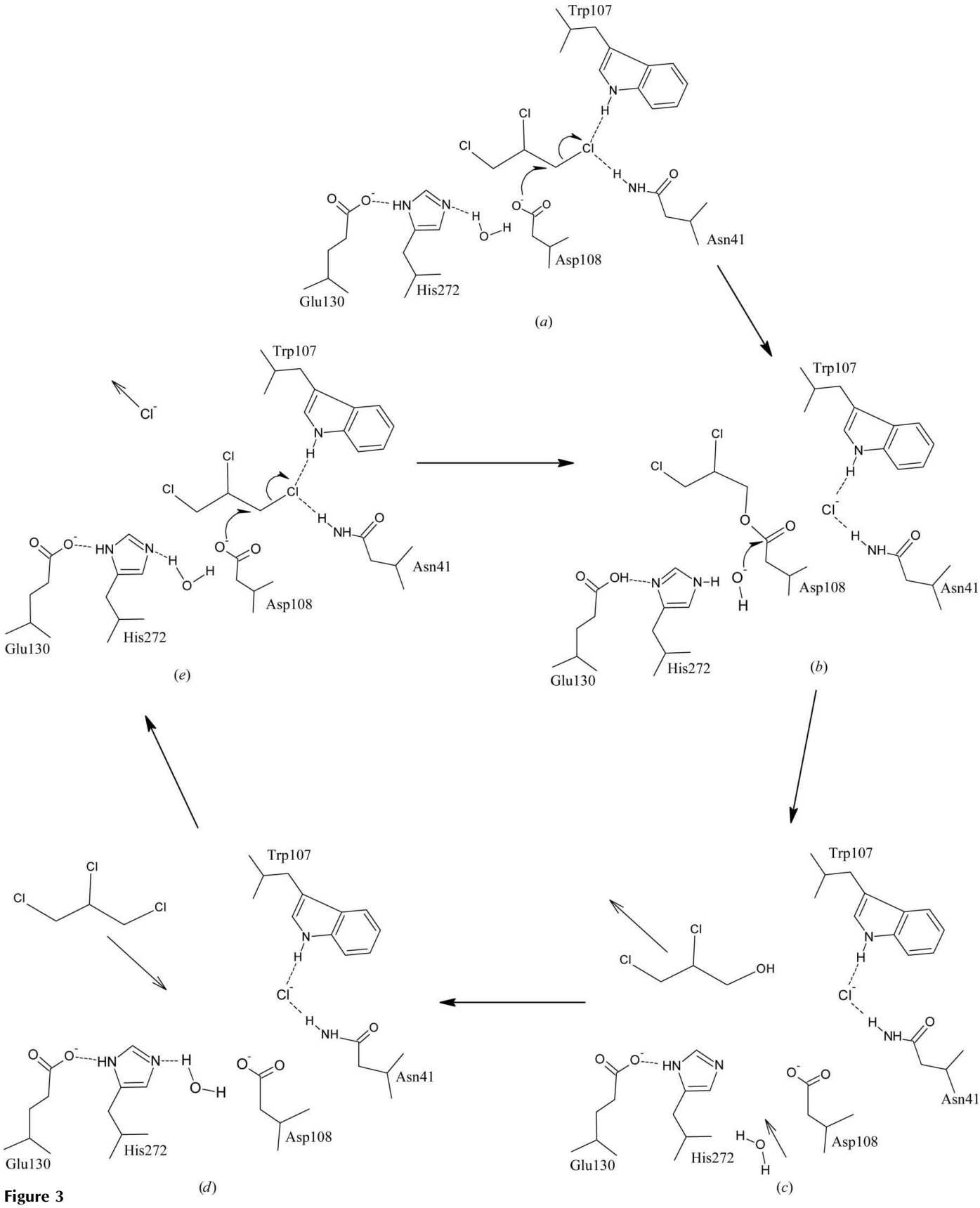

Figure 3
Proposed reaction mechanism of DhaA from *R. rhodochrous* (based on Verschueren, Seljée *et al.*, 1993). The reaction schema is as follows. (*a*) Substrate binding and nucleophilic attack of Asp106. (*b*) Alkyl-enzyme intermediate followed by nucleophilic attack of water. (*c*) The halogen remains bound to the catalytic residues Asp106 and His272, the alcohol product leaves the active site and a new hydrolytic water enters the active site. (*d*) A new substrate molecule (pre-attack or near-attack orientation) enters the active site and (*e*) replaces the chloride ion in the canonical halide-binding site.

and Trp107 side chains (canonical halide-binding site), and the substrate presumably resides in a pre-attack or near-attack orientation. During initial modelling of the TCP substrate, alkyl-enzyme and 2,3-dichloropropane-1-ol product, we noticed that the three Cl atoms of 1,2,3-trichloropropane also superimposed correctly with the $F_o - F_c$ difference electron-density peak at the halide-binding site and two of the three $F_o - F_c$ difference electron-density peaks used in the modelling of the TCP molecule in the pre-attack or near-attack orientation. However, the modelling of this TCP orientation was abandoned because of a negative $F_o - F_c$ difference electron-density peak at one of its C atoms. Nonetheless, from the model it became clear that the relocation of one particular Cl atom is sufficient to switch from the pre-attack or near-attack orientation to the proper orientation necessary for catalysis to proceed.

The second state is characterized by a conformation of the Asp106 side chain (alternative *B*, occupancy of 0.4) ready to perform a nucleophilic attack on the C atom of a bound substrate molecule (Figs. 3*a* and 3*e*). Compared with the first state, the distance between the $O^{\delta1}$ atom of Asp106 and the $N^{\varepsilon2}$ atom of His272 changes from 2.53 to 3.14 Å. Here, the catalytic water molecule (H_2O-1; occupancy of 0.4) is located 2.76 Å away from the C^{γ} atom of Asp106, 3.17 Å from the $N^{\varepsilon2}$ atom of His272 and 2.59 Å from the carbonyl O atom of Asn41. These observations are consistent with the interactions described by Verschueren, Seljée *et al.* (1993). The chloride ion bound in the canonical halide-binding site is a product formed during the reaction that will be replaced by a substrate molecule to start the next reaction cycle (Figs. 3*d* and 3*e*). Furthermore, three chloride ions with partial occupancies were modelled in noncanonical halide-binding positions, revealing a possible route for halide release in the DhaA31 variant (Fig. 4). These noncanonical halide-binding sites, which were not observed in wild-type DhaA, are close to the V245F, C176Y and Y273F mutations located at the mouth of the main tunnel. These substitutions play a crucial role in the reshaping of the DhaA hydrophobic pocket. Consequently, the volume of the active site of DhaA31 (127 Å^3) is clearly reduced in comparison to that of wild-type DhaA (187 Å^3). When it is taken into account that a TCP molecule has a calculated volume of 105 Å^3, the variant DhaA31 has an active site complementary for a TCP molecule, leaving little space for water solvent. The bottlenecks of both the main and side access tunnels are also significantly altered in DhaA31. Reduced accessibility of the active site to water molecules, promoting the formation of the activated complex, has previously been proposed as a key mechanism for the improved activity of DhaA31 towards TCP (Pavlova *et al.*, 2009).

4. Conclusions

Crystals of DhaA31 were obtained in two different forms: (i) a substrate-free form and (ii) a form in complex with 1,2,3-trichloropropane (occupancy of 0.6). The crystal structures provide new information on certain stages of the catalytic cycle of the enzyme. Most interestingly, the catalytic residue Asp106 displays two alternative conformations. Conformation *A* represents a post-attack conformation of Asp106 with the catalytic His272 protonated, creating a salt bridge to the nucleophile at low pH (Verschueren, Kingma *et al.*, 1993*a*; Verschueren, Seljée *et al.*, 1993). The alternative conformation *B* is observed as a result of the loss of the salt bridge between the latter two catalytic residues. The water molecule (H_2O-1) located close to the base His272 (at a distance of 3.17 Å) and the C^{γ} atom of the nucleophile Asp106 (at a distance of 2.76 Å for conformation *B*) most probably serves as the catalytic water for cleavage of the alkyl-enzyme bond. The absence of a catalytic water near Asp106 in the post-attack conformation indicates that the hydrolysis of a covalent alkyl-enzyme bond intermediate has taken place (Fig. 2*c*). After hydrolysis of the covalently bound intermediate, another water molecule should relocate to occupy the vacant catalytic water site (for example, H_2O-2; Figs. 2*c*, 2*d* and 3*d*).

Comparative analysis of the wild-type DhaA structure and the DhaA31–substrate complex structure revealed differences in the architecture of the hydrophobic cavity and the two access tunnels. The introduced substitutions, which are mainly located distally from the catalytic residue Asp106, lead to a

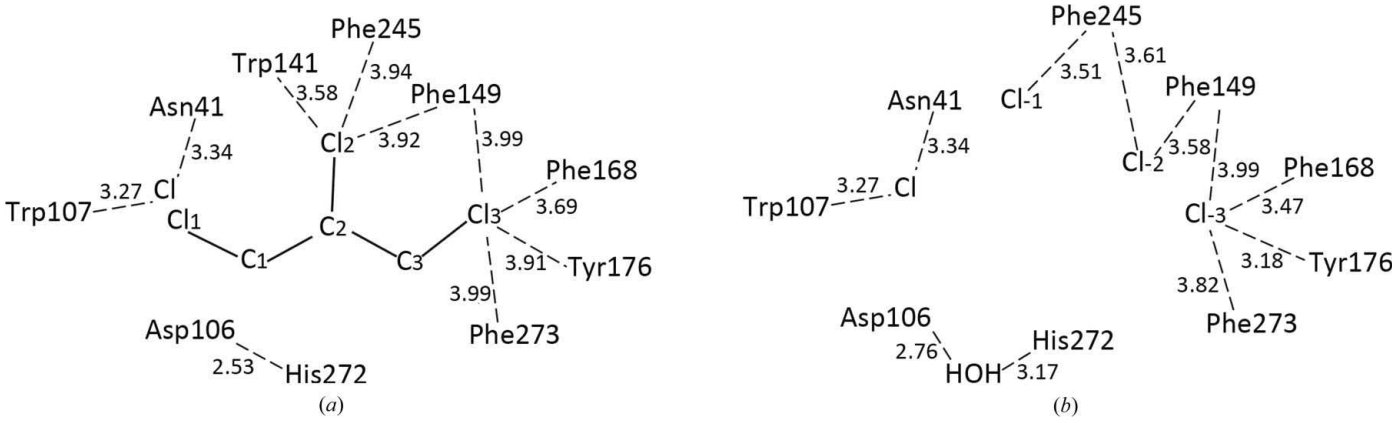

Figure 4
Schematic representation of the DhaA31 hydrophobic cavity: the interaction of hydrophobic residues with the substrate TCP (*a*) and the chloride product (*b*).

reduction in the volume of the hydrophobic pocket and decrease the bottlenecks of the access tunnels. In conjunction with the pH of the crystallization drop and the gentle vapour diffusion of TCP, an enzyme–substrate complex could be obtained. Upon entering the active site of DhaA31, TCP has less available space and binds in a defined manner proximal to Asp106. The defined binding results from specific interactions between the Cl atoms of the substrate on the one hand and Phe149, Phe168, Phe245, Phe273 and Trp141 on the other (Fig. 4*a*).

In our opinion, the observed pre-attack or near-attack orientation of TCP in the complex in the absence of water molecules is a crucial first step in the enhanced catalysis by DhaA31. The hydrophobic pocket of wild-type DhaA is larger and significantly more accessible to solvent water, which may explain the low turnover. For the reaction to proceed in DhaA31, the relocation of one particular TCP Cl atom is sufficient to switch from the observed pre-attack or near-attack state to the proper conformation necessary for catalysis, *i.e.* an obligatory exchange through competition of the chloride ion bound to the canonical halide-binding site between Asn41 and Trp107 and a Cl atom of the substrate is required. The small $F_o - F_c$ difference electron-density peaks distal from Asp106 as observed in the different structures may possibly underscore the role of the main tunnel in substrate and product exchange. This would be in good agreement with a previous study of the product-release pathways, in which the insertion of bulky residues into two access tunnels of wild-type DhaA decreased the accessibility of the individual tunnels to halide ions and alcohol products (Klvana *et al.*, 2009).

In summary, vapour soaking of DhaA31 with 1,2,3-trichloropropane at pH 6.5 facilitated the production of an enzyme–substrate complex, revealing two alternative conformations of the nucleophilic residue Asp106. The low pH contributed to retention of the chloride product at different positions inside the new hydrophobic pocket, illustrating a possible trajectory for chloride-ion release through the main tunnel. Comparative analysis of three crystal structures provided information on the possible structural basis of the enhanced conversion of TCP by DhaA31, which is owing to a reduced volume and redesign of the active-site pocket.

We thank the staff at EMBL (DESY, Hamburg) and BESSY (Berlin) for assistance with data collection, as well as Rolf Hilgenfeld (University of Lübeck) for enabling and arranging a short-term laboratory visit. This work was supported by the Grant Agency of the Czech Republic project P207/12/0775. Support of the Ministry of Education of the Czech Republic and the Academy of Sciences of the Czech Republic is also appreciated.

References

Banás, P., Otyepka, M., Jerábek, P., Petrek, M. & Damborský, J. (2006). *J. Comput. Aided Mol. Des.* **20**, 375–383.
Bosma, T., Damborský, J., Stucki, G. & Janssen, D. B. (2002). *Appl. Environ. Microbiol.* **68**, 3582–3587.
Bosma, T., Kruizinga, E., de Bruin, E. J., Poelarends, G. J. & Janssen, D. B. (1999). *Appl. Environ. Microbiol.* **65**, 4575–4581.
Chen, V. B., Arendall, W. B., Headd, J. J., Keedy, D. A., Immormino, R. M., Kapral, G. J., Murray, L. W., Richardson, J. S. & Richardson, D. C. (2010). *Acta Cryst.* D**66**, 12–21.
Chovancová, E., Kosinski, J., Bujnicki, J. M. & Damborský, J. (2007). *Proteins*, **67**, 305–316.
Ducruix, A. & Giegé, R. (1999). Editors. *Crystallization of Nucleic Acids and Proteins: A Practical Approach*, 2nd ed. Oxford University Press.
DeLano, W. L. (2002). *PyMOL*. http://www.pymol.org.
Emsley, P., Lohkamp, B., Scott, W. G. & Cowtan, K. (2010). *Acta Cryst.* D**66**, 486–501.
Engh, R. A. & Huber, R. (1991). *Acta Cryst.* A**47**, 392–400.
Engh, R. A. & Huber, R. (2001). *International Tables for Crystallography*, Vol. *F*, edited by M. G. Rossmann & E. Arnold, pp. 382–392. Dordrecht: Kluwer Academic Publishers.
Gray, K. A., Richardson, T. H., Kretz, K., Short, J. M., Bartnek, F., Knowles, R., Kan, L., Swanson, P. E. & Robertson, D. E. (2001). *Adv. Synth. Catal.* **343**, 607–617.
Holmquist, M. (2000). *Curr. Protein Pept. Sci.* **1**, 209–235.
Janssen, D. B., Dinkla, I. J. T., Poelarends, G. J. & Terpstra, P. (2005). *Appl. Environ. Microbiol.* **7**, 1868–1882.
Kabsch, W. (1993). *J. Appl. Cryst.* **26**, 795–800.
Kabsch, W. (2010*a*). *Acta Cryst.* D**66**, 125–132.
Kabsch, W. (2010*b*). *Acta Cryst.* D**66**, 133–144.
Klvana, M., Pavlova, M., Koudelakova, T., Chaloupkova, R., Dvorak, P., Prokop, Z., Stsiapanava, A., Kuty, M., Kuta-Smatanova, I., Dohnalek, J., Kulhanek, P., Wade, R. C. & Damborsky, J. (2009). *J. Mol. Biol.* **392**, 1339–1356.
Kulakova, A. N., Larkin, M. J. & Kulakov, L. A. (1997). *Microbiology*, **143**, 109–115.
Lahoda, M., Chaloupkova, R., Stsiapanava, A., Damborsky, J. & Kuta Smatanova, I. (2011). *Acta Cryst.* F**67**, 397–400.
Monincová, M., Prokop, Z., Vévodová, J., Nagata, Y. & Damborsky, J. (2007). *Appl. Environ. Microbiol.* **73**, 2005–2008.
Mueller, U., Darowski, N., Fuchs, M. R., Förster, R., Hellmig, M., Paithankar, K. S., Pühringer, S., Steffien, M., Zocher, G. & Weiss, M. S. (2012). *J. Synchrotron Rad.* **19**, 442–449.
Mueller-Dieckmann, C., Panjikar, S., Tucker, P. A. & Weiss, M. S. (2005). *Acta Cryst.* D**61**, 1263–1272.
Murshudov, G. N., Skubák, P., Lebedev, A. A., Pannu, N. S., Steiner, R. A., Nicholls, R. A., Winn, M. D., Long, F. & Vagin, A. A. (2011). *Acta Cryst.* D**67**, 355–367.
Newman, J., Peat, T. S., Richard, R., Kan, L., Swanson, P. E., Affholter, J. A., Holmes, I. H., Schindler, J. F., Unkefer, C. J. & Terwilliger, T. C. (1999). *Biochemistry*, **38**, 16105–16114.
Oakley, A. J., Klvana, M., Otyepka, M., Nagata, Y., Wilce, M. C. J. & Damborský, J. (2004). *Biochemistry*, **43**, 870–878.
Otwinowski, Z. & Minor, W. (1997). *Methods Enzymol.* **276**, 307–326.
Otyepka, M., Banáš, P., Magistrato, A., Carloni, P. & Damborský, J. (2007). *Proteins*, **70**, 707–717.
Pavlova, M., Klvana, M., Prokop, Z., Chaloupkova, R., Banas, P., Otyepka, M., Wade, R. C., Tsuda, M., Nagata, Y. & Damborsky, J. (2009). *Nature Chem. Biol.* **5**, 727–733.
Pries, F., van den Wijngaard, A. J., Bos, R., Pentenga, M. & Janssen, D. B. (1994). *J. Biol. Chem.* **269**, 17490–17494.
Pries, F., van der Ploeg, J. R., Dolfing, J. & Janssen, D. B. (1994). *FEMS Microbiol. Rev.* **15**, 279–295.
Schindler, J. F., Naranjo, P. A., Honaberger, D. A., Chang, C.-H., Brainard, J. R., Vanderberg, L. A. & Unkefer, C. J. (1999). *Biochemistry*, **38**, 5772–5778.
Sheldrick, G. M. (2008). *Acta Cryst.* A**64**, 112–122.
Stsiapanava, A., Chaloupkova, R., Fortova, A., Brynda, J., Weiss, M. S., Damborsky, J. & Kuta Smatanova, I. (2011). *Acta Cryst.* F**67**, 253–257.
Stsiapanava, A., Dohnalek, J., Gavira, J. A., Kuty, M., Koudelakova, T., Damborsky, J. & Kuta Smatanova, I. (2010). *Acta Cryst.* D**66**, 962–969.
Teng, T.-Y. (1990). *J. Appl. Cryst.* **23**, 387–391.

Vagin, A. & Teplyakov, A. (2010). *Acta Cryst.* D**66**, 22–25.
Vaguine, A. A., Richelle, J. & Wodak, S. J. (1999). *Acta Cryst.* D**55**, 191–205.
Verschueren, K. H. G., Kingma, J., Rozeboom, H. J., Kalk, K. H., Janssen, D. B. & Dijkstra, B. W. (1993*a*). *J. Mol. Biol.* **232**, 856–872.
Verschueren, K. H. G., Kingma, J., Rozeboom, H. J., Kalk, K. H., Janssen, D. B. & Dijkstra, B. W. (1993*b*). *Biochemistry*, **32**, 9031–9037.
Verschueren, K. H. G., Seljée, F., Rozeboom, H. J., Kalk, K. H. & Dijkstra, B. W. (1993). *Nature (London)*, **363**, 693–698.
Voss, N. R. & Gerstein, M. (2010). *Nucleic Acids Res.* **38**, W555–W562.
Winn, M. D. *et al.* (2011). *Acta Cryst.* D**67**, 235–242.